

RADIATION HARDNESS OF SILICON DETECTORS FOR APPLICATIONS IN HIGH-ENERGY PHYSICS EXPERIMENTS

E. Fretwurst, M. Kuhnke, G. Lindström, M. Moll^a

II. Institute for Experimental Physics, University of Hamburg, Germany

^aCERN-EP, Geneva, Switzerland

An overview of the radiation damage induced problems connected with the application of silicon particle detectors in future high-energy physics experiments is given. The present knowledge on the deterioration of the detector performance caused by irradiation with neutrons and high energetic protons is described leading to an appropriate modeling of the macroscopic parameters under irradiation, i.e. increase of the generation current, change of the effective space charge density and degradation of the charge collection efficiency. Possible ways are out-lined for improving the radiation tolerance of silicon detectors either by operational conditions, device optimization or defect engineering by oxygen enrichment of the high resistivity silicon material. Recent results on the effect of oxygen with concentrations in the order of 10^{17} cm^{-3} on the radiation induced changes of the macroscopic parameters and the introduction rate of defects as well as their kinetics measured by DLTS- methods will be presented and discussed in detail.

Keywords: Silicon detectors, Radiation damage, Defects

1. Introduction

Silicon pixel and microstrip detectors have been selected as best choice for most tracking applications in the forthcoming LHC experiments. However the required ten years of safe operability poses an extreme challenge to their radiation hardness, mostly due to the hadron induced damage in the silicon bulk. The ROSE collaboration CERN-RD48 [1] is concentrating on these problems, performing systematic investigations of all detector relevant effects, including the search for an improved radiation tolerance by special defect engineering methods. The main scientific results are outlined, of which the following two points are of major importance: Oxygen enrichment of the silicon bulk, during the manufacturing process, introduced by RD48, has resulted in substantial radiation hardening of the devices. Secondly, a model description has been developed allowing reliable predictions of the detector performance for the LHC operational scenario. Based on these results recommendations are outlined concerning the choice of material and detector processing for silicon detectors for the tracking areas. This technique has been successfully transferred to several manufacturers and test devices for the LHC experiments are presently under study in close cooperation with RD48. In addition, considerable progress has been achieved in the understanding of the microscopic processes responsible for the observed effects in detector performance [2-4].

2. Defect engineered silicon

The key idea of the RD48 strategy is that one can improve the radiation tolerance of silicon by defect engineering. Defect engineering involves the deliberate addition of impurities to silicon in order to affect the formation of electrically active defect centres and thus control the macroscopic parameters of devices. According to current models, RD48 had relied on oxygen and carbon as the key ingredients for a possible change of the radiation hardness. Oxygen and carbon capture silicon vacancies and interstitials, respectively. The carbon is transferred from a substitutional to an

interstitial position, mobile at room temperature. It eventually forms stable defects with oxygen and substitutional carbon. Migrating silicon interstitials and vacancies escape from a region of silicon, where a high concentration of Frenkel pairs is produced by a Primary Knock-On Atom (PKA). The PKA is produced by an incident hadron. Vacancies and interstitials can react with each other, leading to clustering of intrinsic defects, especially at the end of the PKA range. This so-called "cluster" region controls many of the electrical parameters of the irradiated silicon detector.

Various types of silicon had been investigated in the past, covering most of the accessible phase space in Carbon and Oxygen concentration, see Fig.1. The important role of Oxygen was first demonstrated by the use of Czochralski (Cz) silicon, where concentrations of up to 10^{18} cm^{-3} are normal. However this material is not available in detector grade quality. ITME in Warsaw achieved an O-concentration of up to $3 \times 10^{17} \text{ cm}^{-3}$, using a gas jet technique during the FZ process. A method resulting in the same enrichment but with a substantially higher cost effectiveness was finally initiated by RD48.

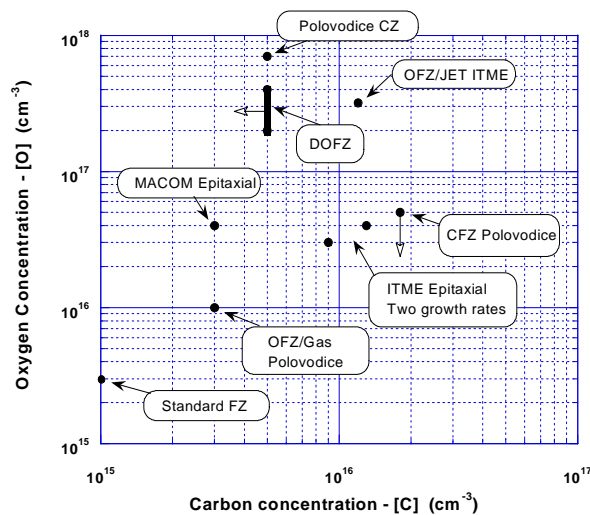


Fig. 1. Oxygen and Carbon concentrations in substrates investigated by the RD48/ROSE Collaboration.

The technique consists of diffusion of oxygen from a thick oxide layer grown via a prolonged oxidation step. Material defect engineered this way is accordingly called DOFZ (diffusion oxygenated float zone) silicon. Only the unexpected results with proton and pion irradiation showed that the oxygenated material is highly superior in radiation tolerance. As the radiation field in the tracking areas of the LHC experiments is dominated by charged hadrons and neutrons play only a significant role at larger radii, with much less intensity, this limitation does not appreciably restrict the benefits of DOFZ silicon detectors. Hence the implementation of the DOFZ technique in the detector processes of manufacturing companies was initiated and meanwhile led to considerable experience.

The proper characterisation of the material before exposing the detectors to radiation was vital for our investigations. Secondary Ion Mass Spectroscopy (SIMS) has proven to be the most reliable technique for evaluating the O-concentration profiles. In Fig. 2 an example is shown comparing the depth profile of Oxygen after standard oxidation with that obtained after prolonged high temperature diffusion.

All material used for the experiments covered in this report is standard FZ silicon of both $\langle 111 \rangle$ and $\langle 100 \rangle$ orientation and resistivity between 1 and 15 $\text{k}\Omega\text{cm}$, supplied by Polovodice, Topsil and Wacker. Most of the work was carried out with special test pad diodes with an area of $5 \times 5 \text{ mm}^2$. The front electrode was surrounded by a single guard-ring, always used as such and laser light injection for special tests was made possible via a small hole in the front electrode and a grid rear electrode. Prior to irradiation the detectors have been fully characterised as to their resistivity and their O- and C-concentration.

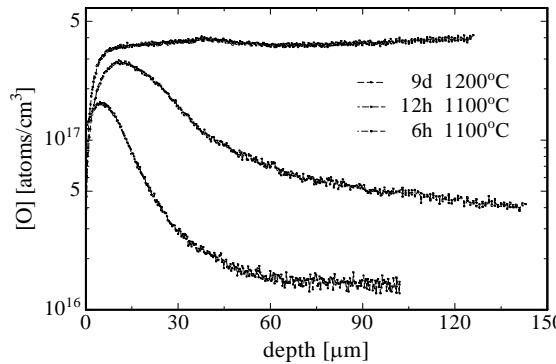


Fig. 2. Oxygen-concentration profiles for standard and oxygen enriched FZ silicon wafers as measured by SIMS.

3. Macroscopic effects

Three main macroscopic effects are seen in high-resistivity diodes following energetic hadron irradiation, these are:

- Change of the doping concentration with severe consequences for the operating voltage needed for total depletion.
- Fluence proportional increase in the reverse current, caused by creation of recombination/generation centres
- Deterioration of charge collection efficiency due to charge carrier trapping leading eventually to a reduction in the signal height produced by minimum ionising particles (mips).

The second and third effects have consequences for the signal-to-noise (S/N) ratio for the detection of mips. However, trapping has been found to be tolerable, and the reverse current can be largely reduced by operating the detectors at a moderately low temperature of about -10°C . The first effect is the most severe, as the operating voltage cannot be increased to very high values. This limitation is predominantly set by the detector processing, but note that a large operating voltage together with the increased reverse current leads also to an increase of dissipation power which may affect the cooling system, and, if distributed non-homogeneously, could also lead to thermal run away effects.

3.1 Scaling of bulk damage with NIEL

The radiation effects to be encountered depend in principal on particle type and energy. Macroscopic changes normally scale with the Non Ionising Energy Loss (NIEL). This scaling has been verified for the reverse current increase, using different types of silicon. Exceptions from this rule have been found when comparing the effect of neutron- and charged hadron damage on the effective doping concentration. However, in order to get a good perception on what could be expected from different particles at different energies, the folding of a given energy distribution with the relevant NIEL function gives quite reliable results. The differences observed from charged or neutral hadrons are then projected onto the parameters describing the radiation effects. A compilation of recommended NIEL values for different particles in the whole relevant energy range is to be found in [5]. It is common practice to represent the intensity of any hadron irradiation by its equivalent fluence of 1 MeV neutrons. All results in this report are given as function of these Φ_{eq} -values.

3.2 Reverse current

The bulk damage induced increase of the reverse current exhibits a simple dependence on particle fluence and temperature. It is entirely due to the generation of electron/hole-pairs at damage

induced defects in the silicon bulk. All detectors have guard-ring structures in order to guarantee a defined value of the sensitive volume V (junction area times detector thickness). With proper use of the guard-ring the reverse current I measured at full depletion is proportional to the volume of the bulk and to the equivalent fluence Φ_{eq} that the detector has received. One therefore defines a *current related damage rate* α by:

$$I = \alpha \cdot \Phi_{eq} \cdot V \quad (1)$$

The measured value of I depends exponentially on the operating temperature in a straight-forward way and according to this all α -values given here are normalised to 20⁰C [6]. Values of the damage rate, measured after 80 min storage of the detectors at 60⁰C, have been found to be largely independent of the individual irradiation history. Using this recipe, comparisons have been made using material of a large variety (conduction type, resistivity, growing technique). The results are displayed in Fig. 3a. The damage induced bulk current undergoes also a temperature dependent beneficial annealing. In Fig. 3b the universal function is given which describes its behaviour. Data measured on oxygenated material do not give any sizeable difference to those measured on standard material. It can therefore be concluded that the damage rate α is independent of any material property, particle type and energy. Hence it may be used to reliably monitor the equivalent fluence of particle sources even in cases of wide energy distributions. The value recommended for this task is the measurement of α in the above described normalised condition, i.e. after 80 minutes annealing at 60⁰C: $\alpha_{80/60} = (3.99 \pm 0.03) \cdot 10^{-17} \text{ Acm}^{-1}$ [6].

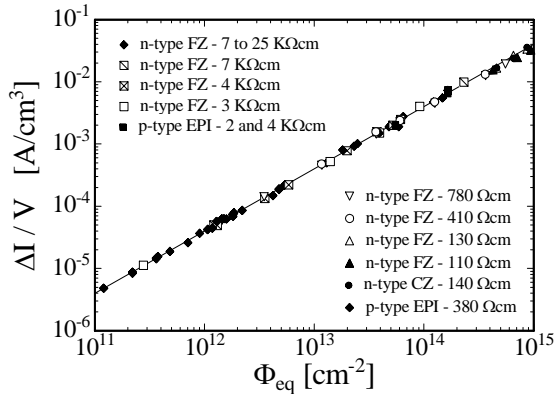


Fig.3a: Fluence dependence of leakage current for detectors produced by various process technologies from different silicon materials. Measured after a heat treatment for 80 min at 60⁰C [6].

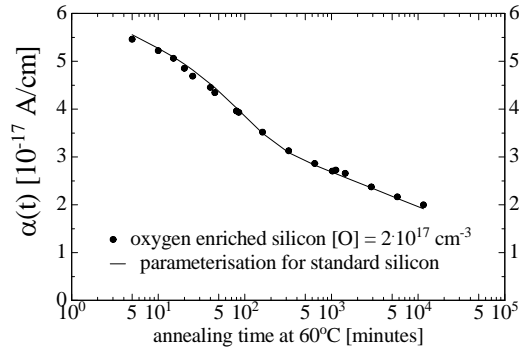


Fig.3b: Current related damage rate α as function of cumulated annealing time at 60⁰C. Comparison between data obtained for oxygen diffused silicon and parameterisation given in Ref. [6].

3.3 Effective doping concentration – depletion voltage

The depletion voltage V_{dep} necessary to fully extend the electric field throughout the depth d of an asymmetric junction diode is related with the effective doping concentration N_{eff} of the bulk by

$$V_{dep} \approx \frac{q_0}{2\epsilon\epsilon_0} |N_{eff}| d^2 \quad (2)$$

This equation holds not only for the original n-type silicon with N_{eff} governed by an abundance of donors but also after severe irradiation when the effective doping concentration changes its sign, due both to a “donor removal” and the increasing generation of acceptor like defects. In any case $|N_{eff}| = |N_d - N_a|$, with N_d being the donor-concentration and N_a that of the acceptors (including charged deep levels).

CERN-scenario measurements for rapid comparison

Although the change of N_{eff} with fluence as well as its annealing behaviour is rather complex (see below), it was found useful to perform rapid comparisons of the radiation hardness almost online during the irradiation experiments. However this can lead to quite large inconsistencies due to the fact that larger fluences can normally only be obtained by longer irradiation. In order to avoid implications produced by simultaneous damage generation and annealing during the irradiation experiment a normalisation recipe had been devised giving results, which are rather independent on the irradiation history. Making use of the fact that the annealing of the damage-induced change of N_{eff} follows a rather flat dependence around 10 days storage at room temperature, corresponding to about 4 minutes at 80°C, a ‘‘CERN scenario measurement’’ technique was devised [7]: After each successive irradiation step the device under test is stored for 4 minutes at 80°C and then the normal C/V technique is used for measuring the depletion voltage. Results of such experiments are shown in Fig. 4a and b. The minimum in these curves for $|N_{eff}|$ is displaying the fluence for which the material becomes type inverted, and the increase at higher fluence values is almost linear. The slope β of this branch is a very good measure of the radiation hardness. Although oxygenated material does not exhibit any benefit for neutron irradiation, it clearly leads to superior results with respect to standard silicon in case of proton or pion induced damage. While the improvement in β is about a factor of 3 an adverse effect is found for Carbon enrichment, see Fig. 4b.

Annealing Measurements and Modelling

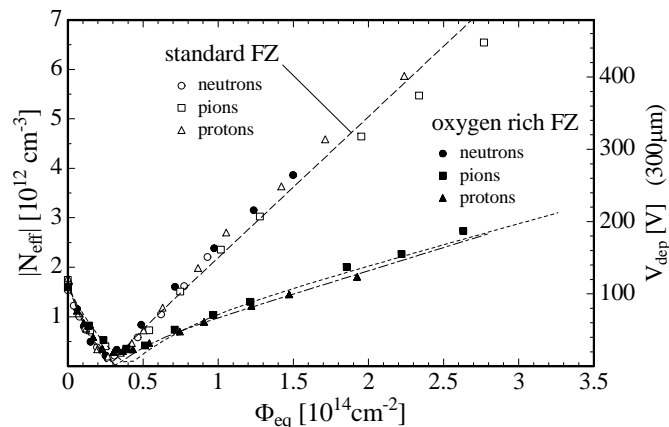


Fig. 4a. Dependence of N_{eff} on the accumulated 1 MeV neutron equivalent fluence for standard and oxygen enriched FZ silicon irradiated with reactor neutrons (Ljubljana), 23 GeV protons (CERN PS) and 192 MeV pions (PSI).

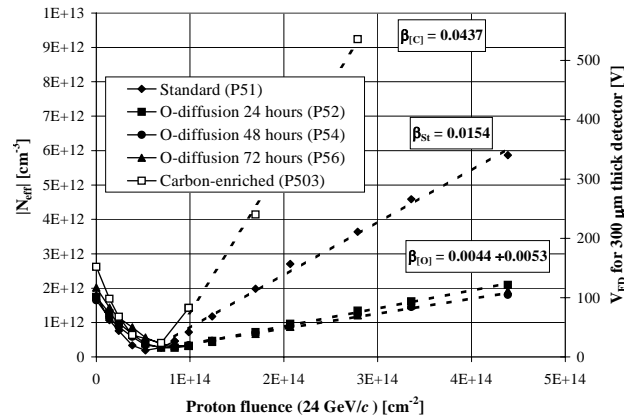


Fig. 4b. Effective space charge density and full depletion voltage versus proton fluence for standard, carbon-enriched and three types of oxygen diffused samples: 24, 48 and 72 hour diffusion at 1150°C.

The CERN-scenario measurements have proven to be extremely useful for a fast damage evaluation of different materials. Only this way was it possible to select the most promising defect engineering process resulting in an appreciable improvement of radiation hardness. However these tests allow the measurement of only one of the relevant parameters, namely the effective doping concentration at or around the minimum of the annealing function. A different approach, introduced by the Hamburg group, uses a set of diodes processed from the same material and individually irradiated at different fluences. Each diode then undergoes a full annealing cycle at an elevated temperature for accelerating the annealing kinetics. This is a time consuming effort but allows the study of all components in the change of the effective doping concentration in a most systematic way. An example of the whole complex behaviour is given in Fig. 5. Here ΔN_{eff} is the damage-induced change in the effective doping concentration with respect to its initial value before irradiation.

$$\Delta N_{eff}(\Phi_{eq}, t(T_a)) = N_{eff,0} - N_{eff}(\Phi_{eq}, t(T_a)) \quad (3)$$

As function of time and fluence ΔN_{eff} can be described as:

$$\Delta N_{eff}(\Phi_{eq}, t(T_a)) = N_A(\Phi_{eq}, t(T_a)) + N_C(\Phi_{eq}) + N_Y(\Phi_{eq}, t(T_a)) \quad (4)$$

In this equation, it has been emphasised that the time dependence is in itself subject to the annealing temperature T_a . As indicated in Fig. 5 and obvious from eq.(4) ΔN_{eff} consists of three components: a short term beneficial annealing N_A , a stable damage part N_C and the reverse annealing component N_Y . N_C can be described by an incomplete “donor removal”, depending exponentially on the fluence, with a final value N_{C0} , and a fluence proportional introduction of stable acceptors, with an introduction rate g_C :

$$N_C(\Phi_{eq}) = N_{C0}(1 - \exp(-c\Phi_{eq})) + g_C\Phi_{eq} \quad (5)$$

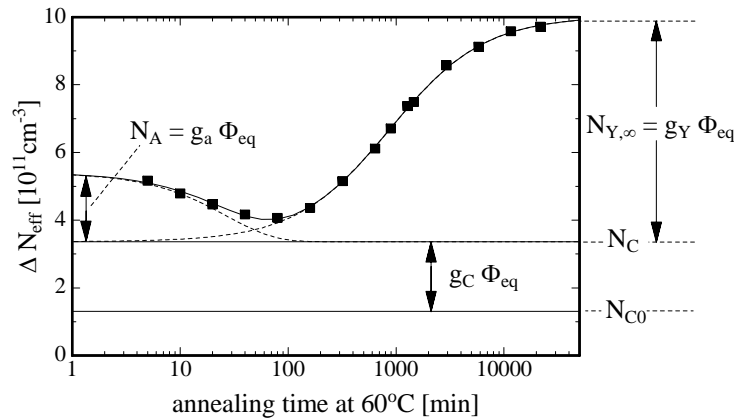


Fig. 5. Annealing behaviour of the radiation induced change in the effective doping concentration ΔN_{eff} at 60°C [6].

Disregarding the presence of a component from the beneficial annealing and a starting reverse annealing part, N_C should obey a very similar dependence on Φ_{eq} as exhibited in the CERN scenario experiments (see Fig. 4) and, hence, there is a close relation between β and g_C , given here. Finally the reverse annealing component is best described by a dependence on annealing time according to $[1 - 1/(1 + t/\tau_Y)]$, where the reverse annealing amplitude is given by $N_Y = g_Y \Phi_{eq}$. It should be noted that this function is practically identical to a 1st order approach according to $[1 - \exp(-t/\tau_Y)]$ for moderately short annealing times but differs appreciably approaching the saturation value. The time constants of the annealing process have been found to be independent of the irradiation fluence, pointing to a first-order process at the microscopic level. Also the temperature dependence of the time constants has

been explored, giving the corresponding activation energies and frequency factors [6]. Having measured these values, one can easily transfer the annealing function obtained at high temperature (for faster measurement) to any given value. With respect to a 20°C measurement this acceleration factor for the reverse annealing is e.g. 550 for an annealing at 60°C.

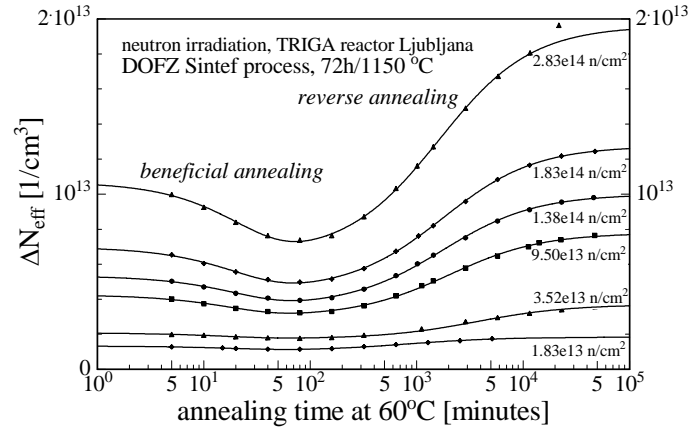


Fig. 6. Systematic analysis of annealing data. Change of effective doping concentration ΔN_{eff} during isothermal annealing at 60°C of oxygen enriched silicon detectors irradiated with different neutron fluences.

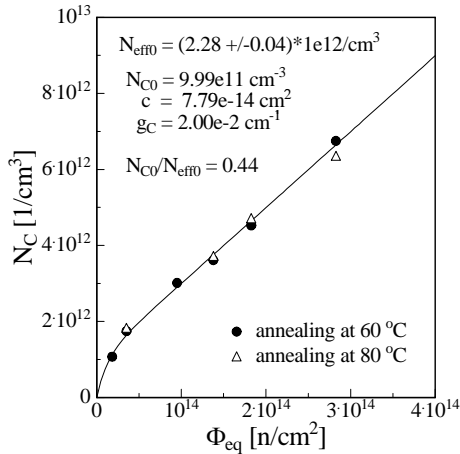


Fig. 7a. Stable damage component N_C for neutron irradiated oxygen enriched silicon.

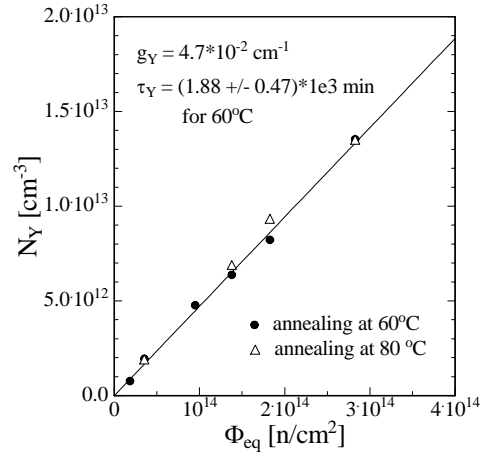


Fig. 7b. Reverse annealing N_Y for neutron irradiated oxygen enriched silicon.

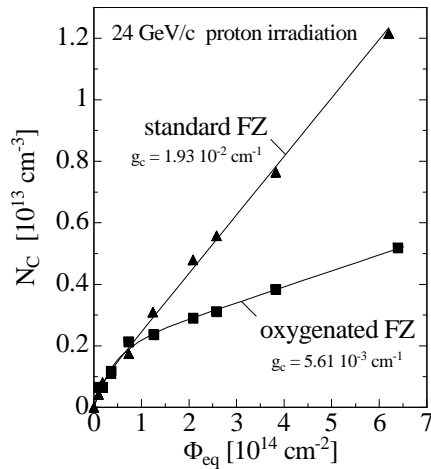


Fig. 8a. Damage parameters N_C for oxygenated and standard material as obtained from annealing experiments at 60°C after irradiation with 24 GeV/c protons.

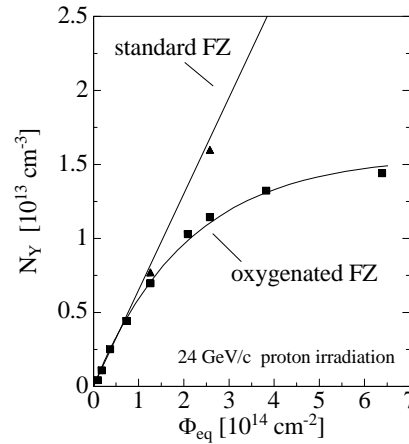


Fig. 8b. Damage parameters N_Y for oxygenated and standard material as obtained from annealing experiments at 60°C after irradiation with 24 GeV/c protons.

How well this model describes the real data obtained for a large set of different fluences and annealing times spanning 4 orders of magnitude, is shown in Fig. 6. Each full line is the result of a fit with the functional dependence as described above. Using such evaluations the different damage parameters, i.e. N_A , τ_A , N_C , N_Y and τ_Y can be derived. As an example the extracted N_C and N_Y values are given in Fig. 7a and b for neutron irradiation and Fig. 8a and b for proton damage. The main results are the following: In case of neutron irradiation the introduction rate g_C for stable acceptors does not depend on the Oxygen concentration; in both cases it is found to be $g_C = 2 \cdot 10^{-2} \text{ cm}^{-1}$. However for proton irradiation this value amounts only to $5.6 \cdot 10^{-3} \text{ cm}^{-1}$ for the DOFZ silicon, i.e. a factor of more than 4 improvement with respect to standard material. For the reverse annealing part as exhibited in Fig. 8b for proton irradiation there is an even larger advantage of DOFZ in comparison to standard silicon. While for standard silicon a linear fluence dependence of N_Y is observed, with an introduction rate of $5 \cdot 10^{-2} \text{ cm}^{-1}$ one gets a saturating function for this component, using oxygenated silicon cutting the net effect of N_Y by a factor of 2 for $\Phi_{eq} = 6 \cdot 10^{14} \text{ cm}^{-2}$. Closely correlated with the N_Y -saturation is the fact that the evaluated time constant for the reverse annealing is appreciably longer too. For the example shown in Fig. 8b, this amounts to a slowing down by a factor of 2.5 in comparison to standard silicon.

4. Projections of damage results to LHC operational conditions

The operational scenario for the silicon tracker in both the ATLAS and CMS experiment foresees that the detectors will be kept cold during the beam periods since only this way the reverse current can be sufficiently reduced. Cooling is also inevitable during the remaining time each year because room temperature storage would lead to an intolerable increase of the depletion voltage due to reverse-annealing. This effect is practically frozen at lower temperature. On the other hand one has to foresee a partial warm up for maintenance which has to be kept as short as possible. To apply the Hamburg model to reliable projections for LHC operation, one has to know the temperature dependence of the involved time constants, especially that for the reverse annealing. Such measurements have been performed so far only with standard silicon detectors. In the following, the same temperature dependence is provisionally assumed also for the oxygenated silicon (checks are under way). Together with the evaluation of the other parameters relevant for the effective doping concentration, respectively the depletion voltage, it is then possible to estimate the behaviour of silicon detectors in different tracking areas over the full experimental LHC period of 10 years. Results are shown as an example for the pixel B-layer of the ATLAS tracker (see Fig. 9), which is the closest to the interaction point ($r = 4\text{cm}$). The extreme advantage of using DOFZ material is apparent. In fact the operation voltage of 600V would limit the usability of standard detectors to only 3 years, while DOFZ detectors would survive almost the full 10 years period.

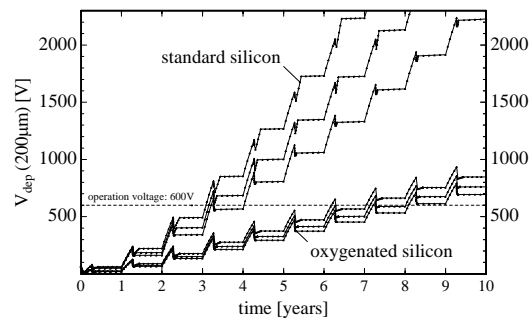


Fig 9. Damage projections for the B-Layer of the ATLAS Pixel Detector for 3 different scenarios per year: a) 100 days beam, detector operated at -7°C , warm up 60 days 20°C ; b) same beam period as given in (a), warm up 30 days 20°C ; c) same beam period (a), warm up 3 days 20°C and 14 days 17°C .

5. Examples of results from microscopic studies

Numerous investigations had been undertaken for defect characterisation in high resistivity silicon, especially by using DLTS (deep level transient spectroscopy) and TSC (thermally stimulated current) techniques [6,8,9], of which only a few examples are given here.

5.1 Spectroscopic defect characterisation

DLTS experiments provide the emission-parameters (activation energy ΔE and cross section σ) and the concentration N_t of all traps within one temperature scan. Traps throughout the entire band gap, except for very shallow levels, can be detected, and majority and minority carrier traps can be distinguished. With some extra effort, the free carrier trapping kinetics (capture coefficients) can be studied. While the trap concentrations derived from DLTS measurements are the most accurate values available compared with all other tools, the most frequently used C-DLTS (capacitance transient DLTS) is strictly limited to trap concentrations well below the doping concentration. For the high-resistivity material studied here this means that the fluence must be very low, orders of magnitude lower than the anticipated during the operation of the detectors. In Fig. 10 we observe all well-known signals from damage-induced defects in silicon and the corresponding isothermal annealing behaviour. Evidently Oxygen and Carbon play an important role as sinks for the primary damage defects (interstitials and vacancies). In fact, the ratio between the C_iC_s and C_iO_i signals in conjunction with their annealing rate can be exploited to determine both the O and C concentrations. The more relevant observations for today's discussion concern the less abundant and unidentified peaks (e.g. H(220K): $E_V + 0.48$ eV), the left and right-hand side broadening of the $VV^{(-/0)}$ transition, and/or the apparent concentration difference between the doubly-charged and singly-charged di-vacancy peak. The two latter observations are currently discussed within the framework of the defect cluster strain model and the "inter-centre charge transfer" model described in refs. [10, 11] respectively.

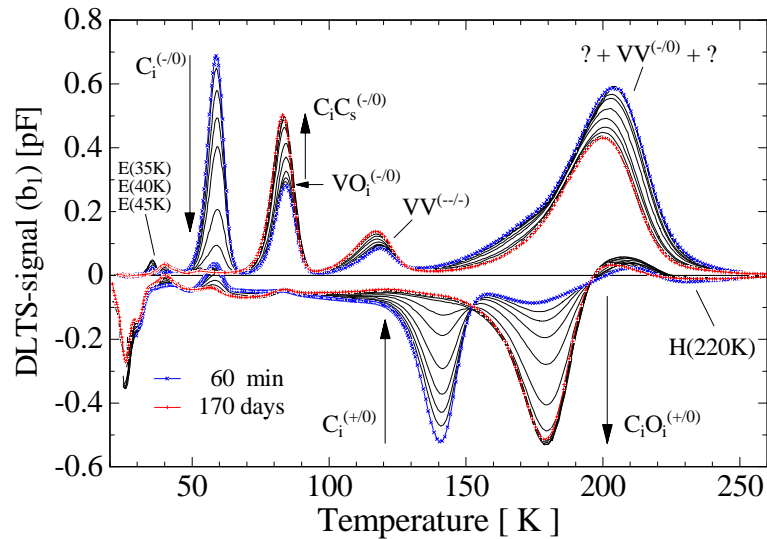


Fig. 10. DLTS-spectrum transformation at room temperature within 170 days after neutron irradiation with $\Phi_{eq} = 2 \times 10^{11} \text{ cm}^{-2}$.

5.2 Influence of oxygen and dependence on particle type

Fig.11 illustrates the influence of the Oxygen content on defect generation. The introduction rate and the shape of the cluster peak at 205 K is found to be independent of the Oxygen concentration. This is expected, as it is known that the leakage current scales very nicely with the concentration of the cluster peak (see §5.3), and that the oxygen content does not affect the leakage current-related damage constant (compare section 3). To a first approximation the generation rate of

VO_i (A-centre) defects does not depend on the oxygen concentration, since under the given irradiation conditions interstitial oxygen is the dominant sink for freely migrating vacancies. It means that VO_i is simply a measure of the total dose. Freely migrating silicon interstitials, on the other hand, are converted into interstitial Carbon, which then has two reaction partners available to form stable defects: substitutional Carbon and interstitial Oxygen. Therefore the ratio between the two resulting reaction products C_iC_s and C_iO_i is proportional to the ratio between C_s and O_i . This explains why for the oxygen-lean material a larger C_iC_s concentration is observed superimposing the VO_i peak.

The dependence of defect generation on the particle type is displayed in Fig. 12. Evidently, the cluster-peak at 205 K is introduced at the same rate in every case, reconfirming the intrinsic nature of the comprising defects and their location within the end-of-range region of the damage cascades. The introduction rate of the isolated point defects, represented by VO_i , C_iC_s , and C_iO_i varies for the different particle types, in agreement with the expected enhancement due to Coulomb scattering (see below). It is interesting to note that in this respect the high-energy (24 GeV/c) protons behave similarly to the 192 MeV pions. Another striking observation concerns the peak normally assigned to the doubly charged di-vacancy. Its variation with particle type resembles the one observed for point defects. Also, the shape of the cluster peak at 205 K does not depend on the particle type. The broadening of the $\text{VV}^{-/0}$ transition and the apparent reduction of the $\text{VV}^{-/0}$ concentration with respect to $\text{VV}^{-/0}$ can therefore not have the same origin. These observations need to be understood in terms of the lattice strain and the “inter-centre charge transfer” models, mentioned above.

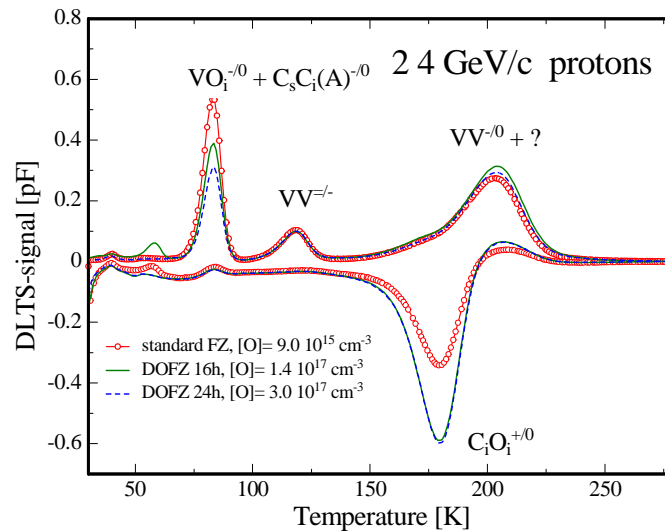


Fig 11. DLTS spectra (normalised to introduction rate at 200K) obtained after irradiation with 24 GeV/c protons and a subsequent 80 min heat treatment at 60°C for different materials (see legend) [12].

5.3 Correlation of defect generation with detector performance

As an example the short term annealing of the leakage current and the effective doping concentration are depicted. It is well known that in both cases the time constants are very similar. Also it is known that the annealing of the right-hand side broadening of the $\text{VV}^{-/0}$ transition, see Fig. 10, correlates with the leakage current annealing. It is therefore tempting to assume that the macroscopic effects have a common cause, namely, the deep level at $E_C - 0.46$ eV, and that this can be reasonably discussed on the grounds of simple Shockley-Read-Hall (SRH) statistics. In order to substantiate this hypothesis, the deep level in question, labelled E4b in the following, was monitored during an isothermal annealing study at 60°C using DLTS, see Fig. 13a. To obtain reliable defect parameters and concentrations for the annealing traps, the difference of two subsequent DLTS spectra was subjected to the standard DLTS evaluation procedure. A very good correlation is observed

between the change in leakage current between two annealing steps and the corresponding change in the concentration of E4b, see Fig. 13b.

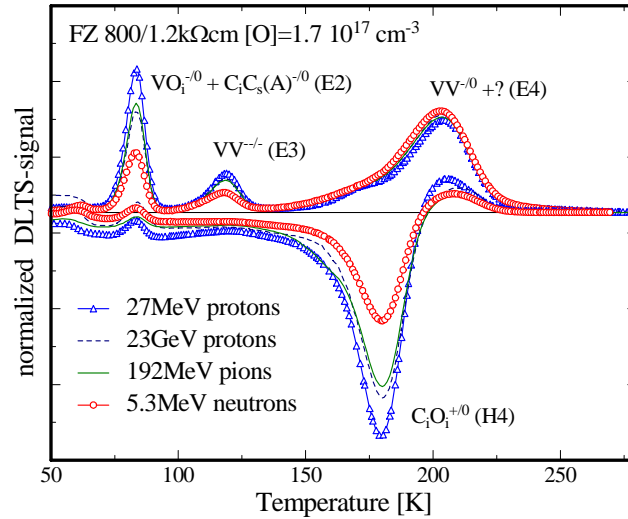


Fig. 12. DLTS spectra obtained on samples from the same wafer obtained after irradiation with different particles (see legend) and a 80 min lasting heat treatment at 60°C. The spectra are normalised to the 1 MeV neutron equivalent introduction rate at 200 K [12].

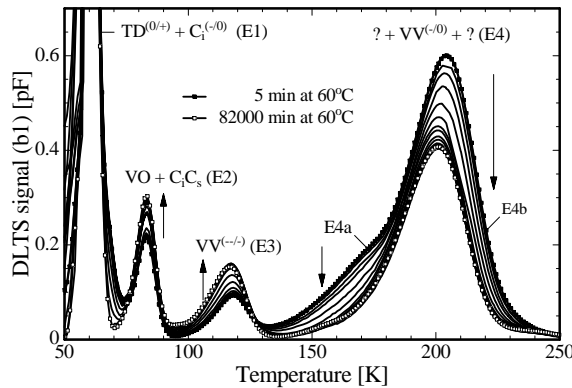


Fig. 13a. Evolution of the DLTS spectrum at 60°C for a neutron irradiated sample (Cz silicon) [12].

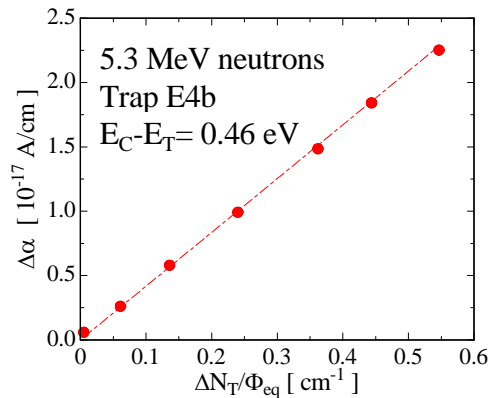


Fig. 13b. Correlation between trap E4b and leakage current [12].

6. Modelling and simulation studies

6.1 Microscopic modelling of detector properties

A key strategy of the ROSE Collaboration has been to understand macroscopic effects by using semiconductor device physics and known microscopic defect concentrations. A further ambitious aim has been to predict defect concentrations using defect kinetics models. This has been discussed in detail in the status reports [2-4]. Here only a brief summary is given on recent modelling results that could explain why oxygen is beneficial to the radiation hardness of silicon when irradiated with protons. The calculations are based on the defect kinetics model described in ref. [13]. Reactions involve all primary products from the initially produced Frenkel pairs (vacancies and silicon interstitials) as well as the major impurities found to be of decisive importance for the damage effects (carbon and oxygen concentration as well as phosphorus as the donor in the initial n-type silicon). The reaction rates of these different interplaying components are controlled by the concentrations of impurities and their relative capture radii. The input parameters required by the model are the oxygen and carbon concentrations (determined by SIMS) and the introduction rates of the primary defects

determined by microscopic measurements as outlined in section 5. Following this modelling the dominant part of the doping changes is expected from the V_2O defect, however there is so far some uncertainty in its energy level. The model predictions coincide rather nicely with experimental findings for gamma-irradiation, if $E_{V_2O} = E_c - 0.54$ eV is assumed, a value which is within the error margin for existing measurements. One can then simply argue that, for gamma irradiated silicon detectors, the use of O-enrichment is beneficial, because the formation of V_2O is suppressed by the competing reaction $V + O \rightarrow VO$, i.e. to say that the possibility for a migrating vacancy to react with VO ($V + VO \rightarrow V_2O$), before it is captured by an interstitial oxygen, is much reduced in comparison to oxygen lean silicon [13].

Unfortunately a similarly simple picture does not hold for hadron irradiation. If the same model is applied the type inversion fluence is an order of magnitude higher than observed experimentally and the leakage current is underestimated by 2 orders of magnitude. The presence of defect clusters in hadron-irradiated material, and their absence in gamma-irradiated material, suggests a possible cause. Several defects are strongly produced within the terminal clusters, including the divacancy (V_2) and their local density might easily be in the order of 10^{19} cm⁻³. Allowing then for possible charge transfer between levels of neighbouring defects (“inter-centre charge transfer”, [11]) indeed leads to a quite reasonable explanation for the high value of the current related damage rate α . The combination of standard SRH calculations for point defects and non standard ones for clusters has also been shown to give relatively good predictions for the observed changes in the effective doping concentration [10]. The difference found in neutron and proton irradiation could then be attributed to the fact that for protons the primary introduction rate of the vacancy is higher than for neutrons (see section 5). Hence, the role of V_2O in determining N_{eff} is greater for protons. As in the case of gamma irradiation, a high oxygen concentration suppresses V_2O production and thus the changes in N_{eff} . Conversely, a high carbon concentration encourages V_2O production because substitutional carbon acts as a sink for interstitials and suppresses capture of interstitials at V_2O ($I + V_2O \rightarrow VO$).

6.2 The NIEL problem

Many experiments have shown that bulk-damage parameters scale independent of particle type and energy with fluence if normalised to the Non-Ionising Energy Loss (NIEL). This important result enables one to extrapolate results obtained with particular sources to the complex particle and energy spectra that will be encountered in the LHC experiments. It was completely unforeseen that this assumption, which had been proven to be valid for standard material, was incorrect for high-energy proton or pion irradiation of oxygen enriched silicon. It has been proposed that the origin of this difference can be understood by a more detailed study of NIEL. Neutrons in the energy range up to several MeV only interact with the silicon by elastic scattering, resulting in relatively high-energy recoil Si-atoms. However, charged hadron interactions incorporate a considerable contribution due to Coulomb scattering resulting in low energy recoils. Assuming that recoil atoms below a certain energy (5 keV) cannot produce defect clusters but predominantly point defects, one would expect that for charged hadrons considerably more of the total NIEL contributes to impurity related defects which indeed leads to the hardening effect of oxygen. This is consistent with results from microscopic studies (section 5), which show that there are more diffusing vacancies and interstitials for protons and pions. Device modelling is also consistent with this hypothesis (section 6.1).

Fig. 14 shows results from a detailed study of the NIEL versus the silicon atom recoil energy for different particles [14]. Only elastic scattering (nuclear + Coulomb) has been included. The relative contribution to NIEL, from recoil energies lower than 5 keV, is negligible for 1 MeV neutrons. But, a considerable portion of the NIEL for charged hadrons exists in that energy range. Elastic scattering of high energy pions or protons contributes only 30 (200 MeV pions) to 37% (9 GeV protons) of the total NIEL and that therefore, according to Fig. 14, the net contribution from recoils below 5 keV is only 6 to 10%. It is hard to believe that this small value could lead to the observed effect. However, for high-energy particles there are many higher order nuclear reactions which lead to a variety of secondary reaction products which again interact with the Si atoms partly by the Coulomb interaction and hence give rise to a significant number of low energy recoils. More detailed investigations using Monte Carlo simulations are presently under way. However one result is already apparent: at high energies, nuclear reactions induced by charged hadrons and neutrons are practically the same. Thus, a

secondary Coulomb contribution to low-energy recoils in the silicon lattice can also be expected, following high-energy neutron damage.

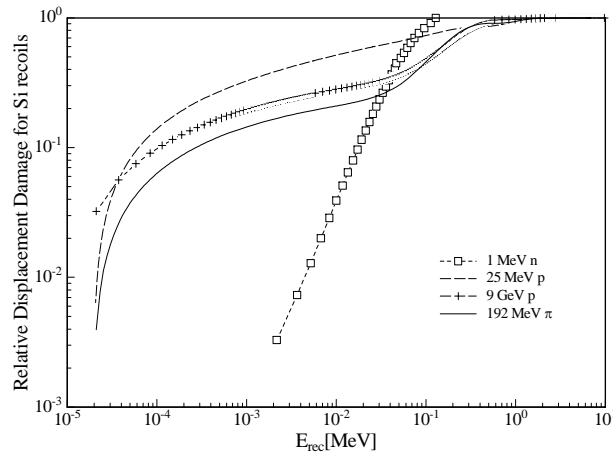


Fig. 14. Relative damage efficiency for different particles as function of recoil energy.

7. Conclusions

The RD48-Collaboration has achieved significant results and reached its original goal to develop radiation hard silicon detectors and provide guidelines to the LHC experiments. The main scientific and technical achievements were:

- The development of an Oxygen enrichment technique in the fabrication of the detector process lead to a major break-through in radiation hardening. This technique has been successfully transferred to several manufacturing companies.
- All relevant macroscopic damage effects have been systematically investigated and reliable parameters for a model description were derived. Projections to LHC experiments have shown substantial advantages for the detector lifetime in the tracking area.
- Microscopic investigations have produced valuable insight in the underlying physics of defect kinetics and model descriptions using their input have shown already a reasonable degree of understanding.

Ongoing work includes the optimisation of the Oxygen enrichment process, some open questions as to the macroscopic and microscopic descriptions and a better understanding of the NIEL problem. The co-operation with the LHC experiments is also pursued concentrating on the comparison between results from the ROSE test pad diodes with those of pixel and microstrip detectors.

Acknowledgements

The authors wish to thank all members of the ROSE collaboration. These results could not have been achieved in a comparatively short time, without their continuous effort.

References

- [1] ROSE-collaboration CERN/RD-48, Proposal for further work on radiation hardening of silicon detectors, CERN/LHCC/97-16&17, (1996).
- [2] RD48 Status report, CERN/LHCC 97-39, June 1997.
- [3] RD48 2nd Status report, CERN/LHCC 98-39, October 1998.
- [4] RD48 3rd Status report, CERN/LHCC 2000-009, December 1999.
- [5] A. Vasilescu in 3rd ROSE Workshop, DESY-Proceedings-1998-02 and A. Vasilescu, G. Lindstroem, Displacement damage in silicon, at <http://sesam.desy.de/~gunnar/>.

- [6] M. Moll, Ph. D. Thesis, Hamburg University, 1999, DESY-THESIS-1999-040, ISSN-1435-8085.
- [7] A. Ruzin, Paper presented on the 8th International Workshop on Vertex Detectors, Texel-Netherlands, 20-25 June (1999).
- [8] H. Feick, Ph. D. Thesis, University of Hamburg, 1997.
- [9] E. Borchi, M. Bruzzi, *La Rivista del Nuovo Cimento della Societa Italiana di Fisica*, **17**(11), (1994).
- [10] B. G. Svensson et al., *Phys. Rev. B*, **43**(3), 2292, (1991).
- [11] S. J. Watts et al., *IEEE Trans. Nucl. Sci.*, **43**(6), 2587, (1996).
- [12] E. Fretwurst et al., paper submitted to the "First International Workshop on Defect Engineering of Advanced Semiconductor Devices" of the ENDEASD, held in Santorini -Greece, 21-22 April 1999, accepted for publication in *Materials Science in Semiconductor Processing*.
- [13] B. C. MacEvoy. PhD thesis, Imperial College, London, November 1996, RAL-TH-07-003.
- [14] A. Vasilescu, G. Lindstroem, M. Huhtinen in Ref. [4].